THE JOURNAL OF BIOLOGICAL CHEMISTRY VOL. 283, NO. 25, pp. 17039–17048, June 20, 2008

The Catalytic Domain of Insulin-degrading Enzyme Forms a Denaturant-resistant Complex with Amyloid β Peptide

*IMPLICATIONS FOR ALZHEIMER DISEASE PATHOGENESIS**[S]

Received for publication, July 31, 2007, and in revised form, April 11, 2008 Published, JBC Papers in Press, April 14, 2008, DOI 10.1074/jbc.M706316200

Ramiro E. Llovera[‡], Matías de Tullio[‡], Leonardo G. Alonso[‡], Malcolm A. Leissring[§], Sergio B. Kaufman[¶1], Alex E. Roher[‖], Gonzalo de Prat Gay[‡1], Laura Morelli[‡1], and Eduardo M. Castaño[‡1,2]

From the [‡]Fundación Instituto Leloir-Instituto de Investigaciones Bioquímicas de Buenos Aires, Consejo Nacional de Investigaciones Científicas y Técnicas (CONICET) , 435 Av. Patricias Argentinas, Ciudad de Buenos Aires C1405BWE, Argentina, the [§]Department of Biomedical Sciences, Scripps Florida, Jupiter, Florida 33458, the [¶]Instituto de Química y Fisicoquímica Biológicas-CONICET and Departamento de Química Biológica, Facultad de Farmacia y Bioquímica, Universidad de Buenos Aires, Buenos Aires, Argentina, and the [‖]Sun Health Research Institute, Sun City, Arizona 85351

Insulin-degrading enzyme (IDE) is central to the turnover of insulin and degrades amyloid β (Aβ) in the mammalian brain. Biochemical and genetic data support the notion that IDE may play a role in late onset Alzheimer disease (AD), and recent studies suggest an association between AD and diabetes mellitus type 2. Here we show that a natively folded recombinant IDE was capable of forming a stable complex with Aβ that resisted dissociation after treatment with strong denaturants. This interaction was also observed with rat brain IDE and detected in an SDS-soluble fraction from AD cortical tissue. Aβ sequence 17–27, known to be crucial in amyloid assembly, was sufficient to form a stable complex with IDE. Monomeric as opposed to aggregated Aβ was competent to associate irreversibly with IDE following a very slow kinetics ($t_{½}$ ~ 45 min). Partial denaturation of IDE as well as preincubation with a 10-fold molar excess of insulin prevented complex formation, suggesting that the irreversible interaction of Aβ takes place with at least part of the substrate binding site of the protease. Limited proteolysis showed that Aβ remained bound to a ~25-kDa N-terminal fragment of IDE in an SDS-resistant manner. Mass spectrometry after *in gel* digestion of the IDE·Aβ complex showed that peptides derived from the region that includes the catalytic site of IDE were recovered with Aβ. Taken together, these results are suggestive of an unprecedented mechanism of conformation-dependent substrate binding that may perturb Aβ clearance, insulin turnover, and promote AD pathogenesis.

Several neurodegenerative disorders are associated with the progressive accumulation of amyloid β (Aβ)[3] in the brain, including Alzheimer disease (AD) (reviewed in Ref. 1). Aβ accumulation has been attributed to several convergent mechanisms. These include a high rate of Aβ production, a fast kinetic of aggregation, and a defective clearance in the brain as the result of impaired transport, protein-protein interactions, or specific protease deficiencies (reviewed in Ref. 1). The first two mechanisms may account for the accelerated Aβ deposition in rare hereditary disorders caused by mutations in the amyloid β precursor protein (APP) or presenilin genes, whereas the latter may be relevant in the complex pathogenesis of the more frequent sporadic AD. It is now accepted that self-assembly of Aβ follows a nucleation kinetic (2). In this process, nucleation takes place above the critical concentration of the peptide, and, therefore, the transient and steady levels of monomeric Aβ in the brain and the mechanisms that regulate them acquire a major importance. Although the input of Aβ depends largely on the rate of proteolytic release from APP, its clearance depends on diffusion, transport, and degradation. Neprilysin, insulin-degrading enzyme (IDE), and endothelin-converting enzyme are thought to be Aβ proteases of major physiological relevance, as shown by gene knock-out and overexpression animal models (3–7). IDE is a highly conserved and ubiquitous Zn^{2+} metalloendopeptidase that belongs to the M16 family defined by an "inverted" canonical sequence in the active site (H*XX*EH instead of HE*XX*H), as compared with other members of the clan (8). Although the precise physiological role of IDE is unknown, its deficiency after gene targeting in mice leads to a biochemical phenotype that includes hyperinsulinemia, glucose intolerance, elevated levels of soluble Aβ in the brain, and a substantial increase in the ~50-residue C-terminal intracellular domain of APP (4, 5). These findings, together with preceding work on cell cultures, support that IDE participates in the degradation of these peptides *in vivo*, regulating their physiological levels (9, 10). In addition, IDE has been shown to

* This work was supported in part by grants from the Alzheimer's Association (to E. M. C.) and the Agencia de Promoción Científica y Tecnológica (to L. M. and E. M. C.). The costs of publication of this article were defrayed in part by the payment of page charges. This article must therefore be hereby marked "*advertisement*" in accordance with 18 U.S.C. Section 1734 solely to indicate this fact.

[S] The on-line version of this article (available at http://www.jbc.org) contains supplemental Figs. S1–S5 and Table S1.

[1] Members of the Consejo Nacional de Investigaciones Científicas y Técnicas.
[2] To whom correspondence should be addressed: Tel.: 54-11-5238-7500; Fax: 54-11-5238-7501; E-mail: ecastano@leloir.org.ar.

[3] The abbreviations used are: Aβ, amyloid β; ACN, acetonitrile; AD, Alzheimer disease; APP, amyloid precursor protein; endo-LysC, endoprotease lysine C; CysC, cystatin C; ELISA, enzyme-linked immunoadsorbent assay; FAβ, fluorescein-labeled Aβ; GRF, growth hormone releasing factor; HCHWA-D, hereditary cerebral hemorrhage with amyloidosis, Dutch type; HFIP, 1,1,1,3,3,3-hexafluoro-2-propanol; HPLC, high performance liquid chromatography; IDE, insulin-degrading enzyme; IDE·AβSCx, IDE·Aβ stable complex; MALDI-TOF, matrix-assisted laser desorption/ionization time-of-flight; PVDF, polyvinylidene difluoride; rIDE, recombinant IDE; TBS, Tris-buffered saline; SB, sample buffer; Tricine, *N*-[2-hydroxy-1,1-bis(hydroxymethyl)ethyl]glycine.

degrade a number of peptides of diverse sequence and functions, including several with the potential to form amyloid *in vivo* or *in vitro*. Apart from insulin, IDE can degrade glucagon, atrial natriuretic peptide, calcitonin, amylin, Aβ, including all its genetic variants, amyloid Bri, and amyloid Dan (reviewed in Refs. 11–13). It has been long proposed that IDE specificity is dictated in part by substrate backbone conformation, a prediction that has been confirmed by recent crystallographic data (11, 14). A growing number of studies suggest a possible genetic association of IDE polymorphisms with sporadic late-onset AD (reviewed in Ref. 15). In addition, recent work supports the association between diabetes mellitus type 2, hyperinsulinemia, and the risk for developing AD, placing IDE as a protein that may link several biochemical features of these diseases (reviewed in Refs. 16 and 17). The expression and activity of IDE have been reported to be reduced in the hippocampus and cortex in sporadic AD and in cortical microvessels affected with amyloid angiopathy (18–20). It has been proposed that part of the loss of IDE activity may be accounted for by lower IDE mRNA levels or post-translational modifications such as oxidative damage (21, 22). In this study we report the unexpected finding that Aβ forms a highly stable complex that comprises part of the active site of IDE, suggesting a novel interaction between IDE and Aβ with potential implications in AD pathogenesis.

MATERIALS AND METHODS

Peptides and Antibodies—Aβ1–28, bovine insulin, bovine ubiquitin, and human growth hormone releasing factor 1–40 (GRF) were from Sigma; Aβ1–40 and Aβ1–42 were from Bachem; Aβ17–40, AβCys16–28, and AβCys17–27 were synthesized at the W. M. Keck facility at Yale University. [^{125}I]Insulin (specific activity, 270 μCi/μg) was a gift of Edgardo Poskus, University of Buenos Aires. Synthetic Aβ1–40E22Q was kindly provided by Dr. Jorge Ghiso (New York University). Human cystatin C (CysC) was from Merck Biosciences. Antibodies against Aβ 6E10 (positions 4–13) and 4G8 (positions 17–24) were from Signet Labs, Dedham, MA. Rabbit polyclonal anti-ubiquitin was from Sigma. The rabbit antisera S40 and S42, specific for Aβ40 and Aβ42, respectively, were gifts of Dr. Mikio Shoji (Okayama University, Japan). Rabbit antiserum BC2 was generated against a glutathione *S*-transferase fusion protein comprising residues 97–273 of rat IDE, as previously described (12). Monoclonal antibody 3A2 against rat IDE was produced and purified as reported previously (20). Rabbit anti-CysC was raised with purified human CysC from urine following standard protocols and characterized by ELISA and Western blot. Human endogenous Aβ1–40 with the E22Q substitution was purified and characterized from the leptomeninges of a case of hereditary cerebral hemorrhage with amyloidosis, Dutch type (HCHWA-D), as previously reported (23).

Fluorescein Labeling of Aβ—AβCys16–28 and AβCys17–27 (1.5 mg/ml) were incubated with a 10-fold molar excess of Tris(2-carboxyethyl)phosphine HCl in 50 mM phosphate, pH 7, for 1 h at room temperature followed by the addition of 60 μl of 2.5 mg of fluoresceinmaleimide (Molecular Probes) in DMSO. The reaction was incubated overnight at 4 °C in the dark and stopped by the addition of β-mercaptoethanol to a final concentration of 50 mM. Peptides were purified by reversed-phase chromatography with a C_{18} column (Beckman Ultrasphere ODS), and the eluate was monitored at 215 nm. HPLC peaks were analyzed by mass spectrometry as described below to assess the incorporation of fluorescein. The peaks containing single peptides with *m*/*z* of 1983.3 and 1726.5, corresponding to fluorescein-labeled AβCys16–28 and AβCys17–27 (FAβs) at a 1:1 stoichiometry, respectively, were identified. The concentrations of these derivatives were determined by absorbance at 492 nm in 0.1 M Tris HCl, pH 9 (extinction coefficient 83,000 cm^{-1} M^{-1}) with a Beckman-Coulter spectrophotometer and stored in the HPLC elution solvent at −80 °C for binding experiments.

Recombinant IDE Purification—Recombinant rat IDE 42–1019 (rIDE) was subcloned from pECE-IDE into pET-30a(+) (Novagen, Darmstadt, Germany), expressed in *Escherichia coli* BL21 and purified using a Hi-Trap Ni^{2+} chelating column as described (20). Further purification was obtained by size exclusion chromatography on a Superdex 200 column (Amersham Biosciences). On-line laser light scattering data were collected with a PD2010 detector. The relation between a 90° static light scattering signal and UV absorbance or refractive index signal was used to calculate molecular mass and hydrodynamic diameter with the Discovery 32 software (Precision Detectors, Bellingham, MA). The purity, folding parameters, and activity of rIDE are shown in supplemental Fig. S1. Protein concentration was determined by absorbance at 280 nm (extinction coefficient, 115,810 cm^{-1} M^{-1}) and by a bicinchoninic acid assay (Pierce) and expressed as monomeric rIDE.

Spectroscopic Studies—CD measurements were carried out on a Jasco J-810 spectropolarimeter. Far-UV spectra were collected using a Peltier temperature-controlled sample holder at 25 °C in a 0.2-cm path length cell, with rIDE concentration of 0.8 μM in 50 mM sodium phosphate, pH 7.2. Fluorescence emission spectra were recorded on an Aminco-Bowman spectrofluorometer with an excitation wavelength of 295 nm in the same buffer and rIDE concentration as above. Denaturation of rIDE induced by urea was assessed by the loss of molar ellipticity at 222 nm and changes in the center of spectral mass of Trp fluorescence at the indicated urea concentrations in the same buffer as above.

rIDE·Aβ Complex Formation and Treatments—Peptides and rIDE were incubated at the indicated concentrations and molar ratios in 0.1 M phosphate, pH 7.2, for 3 h at 37 °C with constant agitation at 350 rpm in a Thermomixer Comfort block (Eppendorf). The reaction was stopped by the addition of an equal volume of 0.25 M Tris-HCl, pH 6.8, 40% glycerol, 4% SDS containing 0.1 M dithiothreitol (sample buffer, SB). To assess the effect of urea and formic acid, the reaction volume was dried under vacuum followed by the addition of 8 M urea in 0.1 M phosphate, pH 7.2, or 70% formic acid, respectively and incubated for 2 h at 37 °C. Acid-treated samples were dried under a stream of N_2 before the addition of electrophoresis SB. For guanidine-HCl treatment, to a 20-μl reaction of rIDE and Aβ1–28, 180 μl of 7.5 M guanidine in HCl (10 mM) or 180 μl of milli-Q water were added, and the samples were incubated for 1 additional hour at 37 °C. After bringing the final volume to 1.8 ml with water, proteins were precipitated with trichloroacetic acid, centrifuged at 15,000 g at 4 °C for 30 min, and carefully washed with ice-chilled acetone to remove the excess of guanidine. This last step was repeated three times. The pellet was

dried under vacuum, and then resuspended with SB for SDS-PAGE and Western blot. Aβ1–40E22Q was incubated at 250 μM in PBS for 3 weeks or applied freshly after disaggregation (see below) for incubation with rIDE. For the time-course experiments, Aβ1–28 was pretreated with 1,1,1,3,3,3-hexafluoro-2-propanol (HFIP) as described (24) and incubated at 100:1 molar ratio (Aβ:IDE) in 20 μl of 0.1 M sodium phosphate, pH 7.2, in the presence or absence of 5 mM EDTA for the indicated times at 37 °C. The reaction was stopped by boiling in 20 μl of SB, and samples were stored at −80 °C until the electrophoresis was performed. Data from two experiments in duplicate were fit to a single exponential equation and analyzed with GraphPad Prism 4 software. Competition experiments were carried out by incubating increasing concentrations of insulin or GRF with 2.5 μM FAβ16–28 and 50 nM rIDE for the indicated periods of time at 37 °C in 0.1 M phosphate, pH 7.2, containing 5 mM EDTA.

Dynamic Light Scattering and Aggregation Assay—Aβ1–28 was pre-treated with HFIP to disaggregate oligomers, dried under nitrogen, dissolved to a final concentration of 100 μM in 0.1 M phosphate, pH 7.2, and filtered through a 0.22-μm membrane. This sample was incubated al 37 °C for up to 72 h, and particle size was assessed at the indicated times by dynamic light scattering using the excitation laser at 633 nm and a detector angle: of 173° with a Zetasizer Nano-S (Malvern Instruments). After the indicated incubation times, data were expressed as particle relative abundance *versus* particle hydrodynamic diameter. To study the aggregation kinetic of FAβCys16–28, the peptide stock was lyophilized, dissolved at the indicated concentrations in 0.1 M phosphate, pH 7.2, and layered upon an equal volume of 20% sucrose in the same buffer. After incubation for the indicated times at 37 °C with continuous agitation at 350 rpm, samples were centrifuged at 10,000 × *g* for 30 min. Aliquots from the supernatant were carefully removed and dissolved in 50 mM Tris-HCl, pH 9, and absorbance was measured at 492 nm. Data from two independent experiments in duplicate were expressed as percentage of soluble peptide, taking the dead time of the experiment as 100%.

IDE·AβSCx Formation with Endogenous IDE—Brains were obtained from adult Sprague-Dawley rats following protocols approved by the Fundación Instituto Leloir Ethical Committee. Tissue was homogenized in Tris-HCl-buffered saline, pH 8 (TBS), containing a mixture of protease inhibitors (Sigma) and centrifuged at 100,000 × *g* for 1 h at 4 °C. One milligram of proteins from the supernatant was immunoprecipitated with monoclonal antibody 3A2 coupled to CNBr-activated Sepharose overnight at 4 °C. After washing with 0.4 M NaCl, 0.1 M Tris-HCl, pH 8, the pellets were incubated with 2 μg of Aβ1–40 in 40 μl of 0.1 M phosphate, pH 8, for 3 h at 37 °C and centrifuged at 3000 rpm for 3 min, and the beads were boiled in 30 μl of SB. Proteins were separated on 7.5% SDS-PAGE and IDE·AβSCx detected by Western blot with antibody S40 as described below. Negative controls included the immunoprecipitation with an unrelated mouse IgG, 3A2-Sepharose beads with buffer alone, and rat brain proteins with protein G alone.

IDE·AβSCx Detection in Rat Brain—The pellet obtained from the rat brain homogenate as described above was homogenized in 10 volumes of TBS containing protease inhibitors, 1% Triton X-100, and 0.1% SDS and centrifuged at 100,000 × *g* for 1 h at 4 °C. One milligram of proteins from the supernatant was immunoprecipitated as indicated before with 3A2 or unrelated mouse IgG in the same buffer without SDS. After washing, proteins were separated on SDS-PAGE and subjected to Western blot with anti-Aβ S40 and S42.

IDE·AβSCx Detection in AD Brain—Brain samples of definite AD cases were obtained from participants enrolled in the Brain Donation Program of Sun Health Research Institute (Sun City, AZ). Approximately 300 mg of frontal cortex from each case was dissected on ice, pooled ($n = 5$), homogenized, and centrifuged as described above. The pellet was homogenized in TBS containing protease inhibitors and 2% SDS and centrifuged at 100,000 × *g* for 1 h at 4 °C. One milligram of proteins from the water and SDS-soluble fractions were used for immunoprecipitation with anti-IDE 3A2 coupled to Sepharose in TBS-0.2% SDS. Proteins were resolved on SDS-PAGE and detected by Western blot using anti-Aβ S42, S40, and BC2 (see below). For urea treatment, the beads pellet was resuspended in 2 vol. of SB containing 9 M urea. Negative controls included immunoprecipitation of brain proteins with an unrelated mouse IgG coupled to Sepharose and 3A2 beads with buffer alone.

High Performance Liquid Chromatography—The separation of rIDE·Aβ complexes by HPLC was performed with a C_4 Brownlee BU-300 (30 × 2.1 mm) column using a linear gradient from 0 to 100% acetonitrile (ACN) in 0.1% trifluoroacetic acid at 0.2 ml/min monitored at 214 nm. The peaks were analyzed by ELISA as described below. For the purification of FAβ peptides, a C_{18} Beckman Ultrasphere (250 × 4.6 mm) was used, with a linear gradient from 0 to 100% acetonitrile in 0.1% trifluoroacetic acid at 1 ml/min. Peaks were detected at 214 nm, collected, and concentrated with a SpeedVac, and peptides were quantitated as described above and analyzed by mass spectrometry (see below). After in gel endoproteinase LysC (endo-LysC) digestion of rIDE·Aβ complex, peptides were separated using a linear gradient from 0 to 100% ACN in 0.1% trifluoroacetic acid in 75 min.

Enzyme-linked Immunoadsorbent Assay—Aliquots of 20 μl from all the peaks obtained from HPLC were mixed with 80 μl of 0.1% trifluoroacetic acid, 50% ACN, placed on polystyrene microtiter plates (Nunc), and incubated at 37 °C until evaporation (typically overnight). After blocking with 3% bovine serum albumin in PBS for 2 h at 37 °C, wells were incubated with antibodies 6E10, 4G8, S40, or BC2 overnight at 4 °C in 0.3% bovine serum albumin in PBS followed by horseradish peroxidase-conjugated anti-mouse or rabbit IgG (Amersham Biosciences) for 2 h at room temperature in the same buffer. Reactivity was developed with *ortho*-phenylenediamine and H_2O_2 for 10 min, stopped with 1 N SO_4H_2, and the optical density was measured at 490 nm with a microtiter plate reader 550 (Bio-Rad, Hercules, CA). After subtraction of background levels (wells without peptide), optical density values were plotted and analyzed with GraphPad Prism version 4. To better reflect the total immunoreactive proteins obtained from each HPLC peak, results were expressed as the product of optical density at 490 nm and peak volume, in arbitrary units.

SDS-PAGE, Western Blot, and Fluorescence Detection—Proteins were run on 7.5 or 12.5% Tris-Tricine gels and transferred to polyvinylidene difluoride (PVDF) membranes. In some experiments, gels were cut horizontally at the level of the

67-kDa molecular mass marker. The lower half was stained with Coomassie Blue, and the upper half was transferred at 400 mA for 3 h to detect rIDE and rIDE·Aβ complexes. Protein complexes formed between rIDE and unlabeled Aβ peptide were detected and quantified by Western blot. Membranes were blocked with 5% low fat milk in PBS for 2 h at 37 °C and with the indicated primary antibodies overnight at 4 °C. Immunoreactivity was detected with anti-rabbit or anti-mouse horseradish peroxidase-labeled IgG and enhanced chemiluminescence using ECL Plus reagents (Amersham Biosciences). Western blots were scanned with a STORM 860 fluorometer and analyzed with ImageQuaNT 5.1 software (Molecular Dynamics). For fluorescence assessment, PVDF membranes were equilibrated in PBS for 45 min, air-dried, and scanned in blue fluorescence mode with the photomultiplier set at 975 V. The intensity of the fluorescent signal as a function of peptide mass was determined by dot-blot on PVDF membranes with FAβs. The amount of total rIDE was estimated by Coomassie Blue staining of the same membranes used for fluorescence detection. For N-terminal sequence, proteins were digested with trypsin at 1:200 for 15 min at room temperature, subjected to SDS-PAGE, and transferred to PVDF. After staining with 0.1% Coomassie Blue the band of interest was cut and subjected to Edman degradation with a 477A sequencer (Applied Biosystems).

In-gel Digestion—After SDS-PAGE and Coomassie Blue staining, the band of 120 kDa containing the rIDE·Aβ (FAβ17–27) complex was cut, and the gel slice was incubated in 100 mM Tris-HCl, pH 8.8 (digestion buffer), with 45 mM dithiothreitol for 30 min at 60 °C. The tube was cooled at room temperature, and 100 mM iodoacetamide was added, followed by incubation for 30 min in the dark at room temperature. The gel was then washed in 50% ACN with shaking for 1 h, cut in 1-mm pieces, and transferred to a small tube. The gel pieces were shrunk in ACN, dried in a rotator evaporator, and re-swollen with 10 μl of digestion buffer containing 0.1 mg/ml endo-LysC (Roche Applied Science). The sample was incubated overnight at 37 °C, and digestion products were extracted twice from the gel with 60% ACN/0.1% trifluoroacetic acid for 20 min. Combined extractions were loaded into a C_{18} HPLC column and separated as described above. Seventy-six 1-min fractions were collected, and volumes were reduced to ~50 μl with a rotator evaporator and applied to a PVDF membrane in PBS for dot-blot fluorescence detection and 4G8 immunoreactivity as described before. Those fractions in which the presence of FAβ17–27 was detected were further analyzed by mass spectrometry. Negative controls included digestion of rIDE alone and a blank piece of gel.

Mass Spectrometry Analysis—FAβ peptides and products of endo-LysC of rIDE in the presence or absence of Aβ were analyzed by matrix-assisted laser desorption/ionization time-of-flight (MALDI-TOF). To produce the dried droplets, a saturated solution of α-cyano-4-hydroxycinnamic acid (Fluka) was prepared using 0.1% trifluoroacetic acid-30% ACN at room temperature. Equal volumes from this solution and the sample were mixed, and 1 μl was placed on the probe, allowed to dry, and analyzed on linear mode in an Omniflex spectrometer (Bruker Daltonics). Calibration was performed with the following peptides for which average *m*/*z* values are shown in parentheses: bradykinin 1–7 (757.86), angiotensin I (1297.49), renin substrate (1760.04), microperoxidase (1862.95), insulin B chain (3496.92), and insulin (5734.54). Peptides were identified with the Flex-Analysis 2.2 software (Bruker), and the Find Pep program available on the ExPASy Proteomic Server. Precision for analysis was set at <0.1%. All the peaks identified as fragments of rIDE were distributed in 100-residue segments of the recombinant enzyme, and the relative frequency for each segment was expressed as the percentage of the total peaks assigned to rIDE.

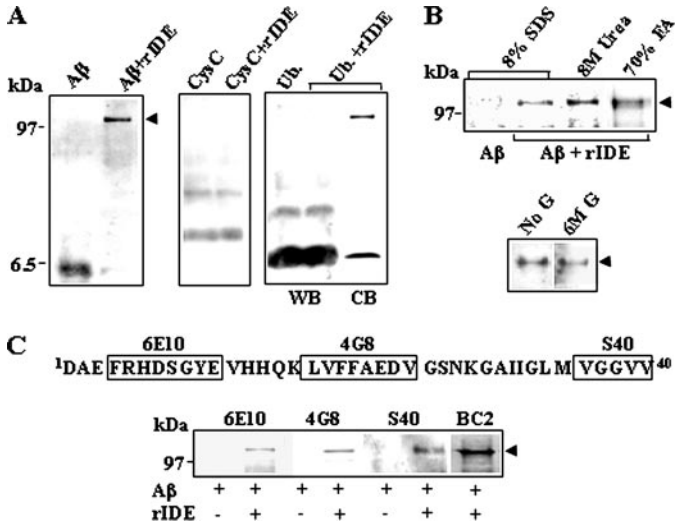

FIGURE 1. *A*, incubation of Aβ1–40 with rIDE results in the formation of an SDS-resistant component. *Left panel*: Western blot with 6E10 monoclonal antibody showing a 120-kDa band after incubation of active rIDE and Aβ (*arrowhead*) that is not present when Aβ was incubated alone. Note that monomeric Aβ was degraded in the presence of rIDE. *Middle* and *right panels*, Western blots (*WB*) of CysC and ubiquitin incubated alone or in the presence of rIDE, respectively. *CB*, Coomassie Blue staining of a gel with the same amounts of ubiquitin and rIDE as shown in the WB. *B*, Western blot with 6E10 of Aβ1–40 alone or preincubated with rIDE after treatment with 8% SDS, 8 M urea, 70% formic acid, or 6 M guanidine-HCl (*G*), respectively. *C*, schematic representation of Aβ1–40 and the epitopes recognized by 6E10, 4G8, and S40 antibodies (*top panel*), and Western blot (*bottom panel*) with the three antibodies showing the 120-kDa component in the presence of rIDE as indicated (*arrow*). BC2 is a polyclonal anti-IDE. On the *left*, in all panels, molecular mass markers in kilodaltons. Representative Western blots from at least two independent experiments are shown.

RESULTS

IDE and Aβ Form a Complex That Resists Dissociation with Strong Denaturants—After incubating synthetic Aβ1–40 (25 μM) with rat rIDE (1 μM), a Western blot with antibody 6E10 specific for Aβ 4–13 showed, in addition to the digestion of the monomeric peptide, a 120-kDa component consistent with a complex between the protease (~115 kDa) and Aβ (~4 kDa). This high molecular weight component was not present when Aβ was incubated alone, ruling out an oligomeric form of the peptide (Fig. 1*A*). The same results were obtained with Aβ1–42 (not shown). No bands in the 120-kDa region were seen when rIDE was incubated with human CysC (11 kDa). As an additional negative control ubiquitin was used, which has been reported to bind and inhibit IDE in a competitive manner (25) (Fig. 1*A*). Remarkably, the 120-kDa component resisted dissociation in the presence of 8% SDS, 8 M urea, 70% formic acid, or 6 M guanidine-HCl at pH 3, indicating its extremely high stability (Fig. 1*B*). The shift in mobility of rIDE upon binding to Aβ was small, consistent with low molecular mass Aβ species as

opposed to large SDS-resistant oligomers associated with rIDE. To explore whether these bound Aβ species were products of proteolysis, the peptide was incubated with rIDE in the presence of 5 mM EDTA. The inhibition of proteolytic activity did not preclude the formation of a stable complex between Aβ and rIDE (IDE·AβSCx). Moreover, monoclonal 4G8 specific for sequence 17–24 (26) and S40, a polyclonal antibody against the C-terminal 5 residues of Aβ1–40 (27), showed the same 120-kDa component as with 6E10 in the presence of EDTA, suggesting that the species associated with rIDE in IDE·AβSCx was intact Aβ1–40 rather than fragments of the peptide (Fig. 1*C*). To study Aβ-rIDE stable association using an entirely different approach, Aβ1–40 and rIDE were incubated and subjected to reversed-phase HPLC. Fractions were analyzed by indirect ELISA using 6E10, 4G8, S40, and BC2 antibodies to follow the elution of Aβ and rIDE, respectively. IDE immunoreactivity was mainly found in one peak (*P2*, Fig. 2*A*), whereas Aβ showed a biphasic pattern, with most of the peptide eluting at *P1* (Fig. 2*A*) and a second, more hydrophobic and smaller peak that eluted together with rIDE in P2. Aβ from P2 reacted on ELISA with 6E10, 4G8, and S40 in accordance with Western blot results suggesting that a full-length peptide was associated with rIDE (Fig. 2*B*). Quantitative estimation by ELISA showed that ~15% of Aβ immunoreactivity co-eluted with the protease. Western blot with 6E10 showed that P1 yielded monomeric Aβ (not shown), whereas P2 contained the SDS-resistant 120-kDa component (Fig. 2*C*).

Endogenous IDE and Aβ Are Capable of Forming IDE·AβSCx—To determine whether endogenous Aβ was capable of forming IDE·AβSCx, we used purified amyloid from the leptomeninges of a case of HCHWA-D. These patients present massive vascular amyloid deposition due to a point mutation in the APP gene resulting in the substitution of Glu for Gln at position 22 of Aβ (E22Q). Aβ Dutch was extracted in 99% formic acid and consisted of a mixture of monomers, dimers, and higher oligomers when analyzed on SDS-PAGE, as previously shown (23). When endogenous Aβ Dutch was incubated with rIDE, Western blot revealed a strong 120-kDa band with 6E10 that was not seen in the absence of rIDE, indicative of IDE·AβSCx (Fig. 3*A*), and that the complex formation observed with synthetic peptides was not an artifact associated with the chemistry of their production. Likewise, endogenous IDE isolated from rat brain formed IDE·AβSCx after incubation with Aβ1–40, indicating that this stable association was not restricted to the recombinant enzyme (Fig. 3*B*). To detect the presence of IDE·AβSCx *in vivo*, a detergent-soluble fraction from adult rat brain was immunoprecipitated with anti-IDE monoclonal 3A2 and analyzed by Western blot with anti-Aβ S40 and S42. A strong immunoreactive band of 120 kDa was seen with both a polyclonal anti-IDE (BC2) and S40 that was absent from the negative controls (Fig. 3*C*). No S42-reactive band was observed (not shown). To extend these results to human brain, water-soluble and SDS-soluble proteins from sporadic AD cortical tissue were immunoprecipitated with anti-IDE monoclonal 3A2. Western blot with anti-Aβ S42, specific for Aβ ending at Ala-42 (27), showed a component of 120 kDa that was not present in the negative controls and resisted incubation in 6 M urea (Fig. 3*D* and supplemental Fig. S2). This band was not detected with S40, possibly due to the overwhelming predominance of Aβ42 over Aβ40 in AD parenchymal deposits (not shown). Remarkably, no IDE·AβSCx was detected in the water-soluble fractions despite a larger amount of immunoprecipitated IDE as compared with the SDS-soluble fraction (supplemental Fig. S2). It is noteworthy that S42 yielded exclusively the typical ladder staining of Aβ oligomers in a direct Western blot of AD brain SDS-soluble proteins, further indicating its specificity (supplemental Fig. S2). Although a definite proof will require direct biochemical characterization after a large scale purification, these results suggest that IDE·AβSCx exists *in vivo* in normal rodent brain and remains associated with amyloid deposits in senile plaques, in accordance with the reported immunohistochemical findings of IDE in AD brains (28).

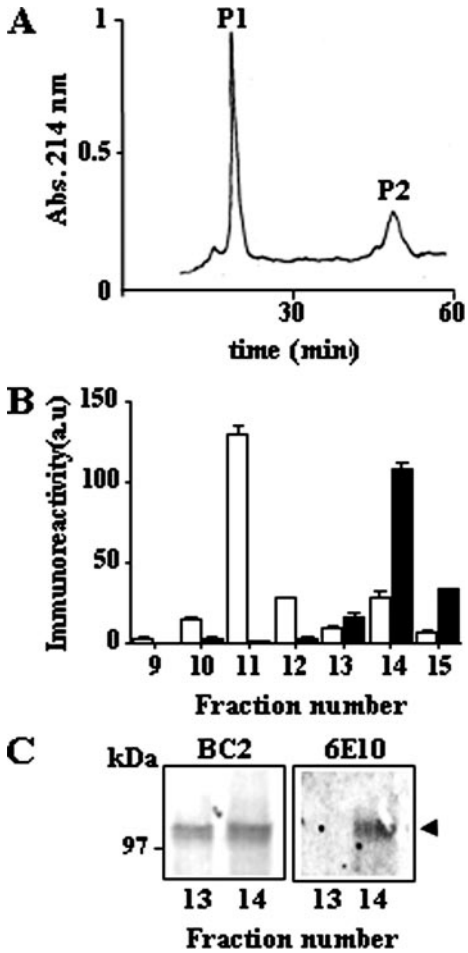

FIGURE 2. *A*, HPLC profile of Aβ1–40 incubated with rIDE as indicated under "Material and Methods" showed two major peaks, *P1* and *P2*. *B*, analysis of the HPLC fractions by indirect ELISA. rIDE immunoreactivity, as detected with BC2 polyclonal antibody (*filled bars*) eluted in *fractions 13–15*, whereas Aβ1–40 eluted mainly in *fraction 11* with a second, minor peak in *fraction 14*, as revealed with monoclonal 6E10 (*open bars*). Data represent the mean ± S.E. of two experiments performed in duplicate. A similar profile was obtained with antibodies 4G8 and S40 (not shown). *C*, Western blot of proteins in *fractions 13* and *14* showed a 120-kDa component that was labeled by 6E10 in the latter only (*arrow*), in agreement with the ELISA results. The *left panel* shows the same membrane stripped and blotted with anti-IDE BC2. Note the slight shift in the molecular mass of the Aβ·rIDE complex. *Left*, molecular mass markers, in kilodaltons.

The Central Region of Aβ Is Sufficient for IDE·Aβ SCx Formation—Major sites of IDE cleavage and all the Aβ pathologic substitutions are clustered within a hydrophobic stretch

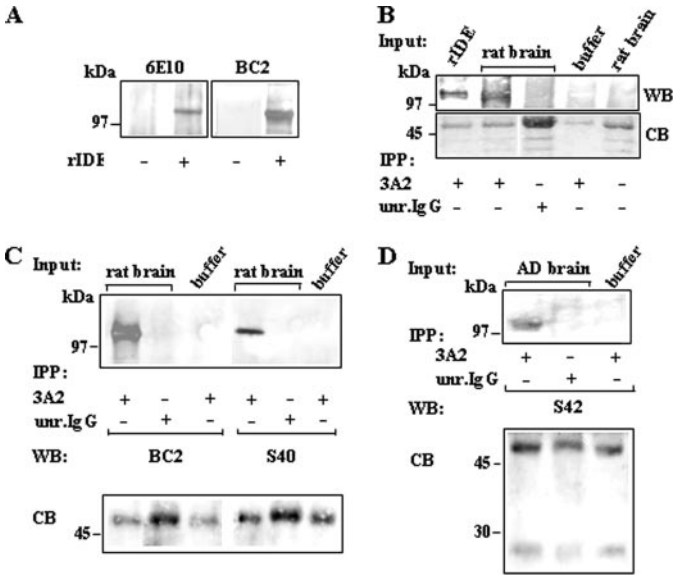

FIGURE 3. *A*, Western blot with 6E10 of Aβ from HCHWA-D leptomeninges incubated in the absence or presence of rIDE. The band of 120 kDa that reacted with both 6E10 and anti-IDE BC2 is seen. *B*, Western blot with S40 antibody of IDE·AβSCx formed between Aβ1–40 and rIDE or endogenous IDE immunoprecipitated (*IPP*) from rat brain with anti-IDE monoclonal 3A2. On *top* of each *lane*, the input for IPP is indicated; *rIDE*, recombinant rat IDE. *WB*, Western blot; *CB*, Coomassie Blue staining of the lower part of the same membrane showing Ig heavy chains. *Unr.IgG*, unrelated mouse IgG. Note that rIDE runs slower (~8 kDa) on SDS-PAGE than endogenous IDE, as described before (20). *C*, *top panel*, *WB* with polyclonal anti-IDE BC2 and anti-Aβ S40 of rat brain proteins after *IPP* with anti-IDE monoclonal 3A2 shows a specific component of 120 kDa consistent with endogenous IDE·AβSCx. *Unr.IgG*, unrelated mouse IgG. *Bottom panel*, the lower part of the membrane was stained with Coomassie Blue (*CB*) to show the Ig heavy chains (*Ig*) of the immunoprecipitates as loading controls. *D*, *top panel*, Western blot (*WB*) with S42 of SDS-soluble proteins form AD cortical tissue after *IPP* with anti-IDE 3A2 shows a specific component of 120 kDa consistent with endogenous IDE·AβSCx. *Unr.IgG*, unrelated mouse IgG. *Bottom panel*, the lower part of the membrane was stained with *CB* to show the Ig heavy and light chains of the immunoprecipitates as loading controls.

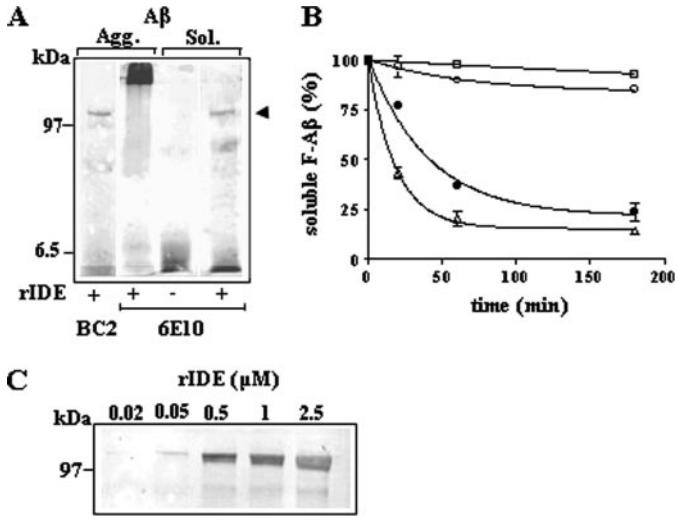

FIGURE 4. *A*, Western blot of pre-aggregated (*Agg.*) or soluble (*Sol.*) Aβ1–40E22Q in the presence or absence of rIDE, as indicated. The 120-kDa component in the presence of rIDE with non-aggregated Aβ is indicated (*arrowhead*). *B*, rate of aggregation of FAβ in 0.1 M phosphate, pH 7.2, as a function of peptide concentration. After incubation, FAβ remaining in the supernatant of 10,000 × *g* was measured at 492 nm at pH 9. 125 nM (□), 250 nM (○), 500 nM (·), and 2.5 μM (△). The mean ± S.E. of two independent experiments performed in duplicate for each condition are shown. *C*, FAβ at 2.5 μM was incubated with increasing concentrations of rIDE as indicated and IDE·AβSCx detected and quantitated as described under "Materials and Methods." There was an increase of ~8-fold in the intensity of the 120-kDa component from 50 to 500 nM of rIDE, where it approached saturation. *Left*, molecular mass markers in kilodaltons. Representative gels of two independent experiments are shown.

between positions 17 and 24 (reviewed in Ref. 1); in addition, this region corresponds to the N terminus of p3, a major product of APP normal processing by α/γ secretases. We next probed shorter synthetic Aβ to test the requirement for this region. The IDE·AβSCx was formed with Aβ1–28 as detected by 6E10 and with AβCys-16–28 and p3 as shown by 4G8 Western blots, respectively (supplemental Fig. S2). Moreover, these components also resisted treatment with denaturants (not shown) indicating that the hydrophobic C terminus of the membrane-embedded domain of Aβ was not necessary for the strong interaction with rIDE. These results also suggested that AβCys16–28 and p3 in IDE·AβSCx were not cleaved, because the linear epitope 17–24 recognized by 4G8 was preserved.

Soluble Aβ Is Competent for the Formation of IDE·AβSCx—We next addressed the question of whether IDE·AβSCx was formed at the expense of soluble or aggregated Aβ. Preincubated Aβ1–40E22Q remained on top of the gel, indicative of extensive aggregation and did not show IDE·AβSCx as opposed to the non-aggregated peptide (Fig. 4*A*). To more accurately quantify rIDE-bound Aβ, AβCys16–28 was labeled with fluoresceinmaleimide (FAβ), purified by HPLC and characterized by MALDI-TOF. A single peak with a mass of 1982.5 was obtained, indicating a 1:1 labeling stoichiometry (not shown). This allowed an estimation of peptide concentration (which lacks Tyr and Trp) by measuring absorbance at 492 nm at pH 9. The derivative FAβ was used to assess aggregation and complex formation with rIDE. As with the unlabeled Aβ peptides, SDS-PAGE showed that FAβ associated into IDE·AβSCx, whereas no stable association was seen with bovine serum albumin or IgG (supplemental Fig. S3). Moreover, FAβ was competed by preincubation with a 10-fold molar excess of unlabeled AβCys-16–28, confirming the specificity of the fluorescent signal (supplemental Fig. S3). Fluorescence intensity in the soluble fraction as a function of concentration and time indicated that FAβ, as expected from previous work (29, 30), readily aggregated above 250 nM after 3 h with continuous agitation at 37 °C (Fig. 4*B*). The fraction of soluble FAβ at steady state was ~20% at 2.5 μM. When FAβ was incubated at 2.5 μM with increasing concentrations of rIDE (50 nM-2.5 μM), the yield of IDE·AβSCx increased ~8-fold up to 500 nM and remained constant to 2.5 μM (expressed in monomers of enzyme) (Fig. 4*C*). A quantitative estimation with dot blots (see supplemental Fig. S3) showed that the maximal amount of FAβ associated with rIDE comprised ~16 ng of FAβ (16% of the total peptide), further supporting that a species of soluble FAβ was limiting for IDE·AβSCx formation under these experimental conditions.

Native IDE·AβSCx Acquires SDS Resistance Very Slowly—Previous work has shown that native endogenous IDE can be isolated by size-exclusion chromatography largely as a dimer (31). Therefore, we subjected rIDE obtained from a Ni^{2+}-affinity column to a Superdex-200 separation under physiological conditions at ~1 μM and obtained a main peak of apparent molecular mass of ~250 kDa (Fig. 5*A*). This component was further characterized by static laser-light scattering as a homogeneous 228-kDa species, consistent with a rIDE dimer (not

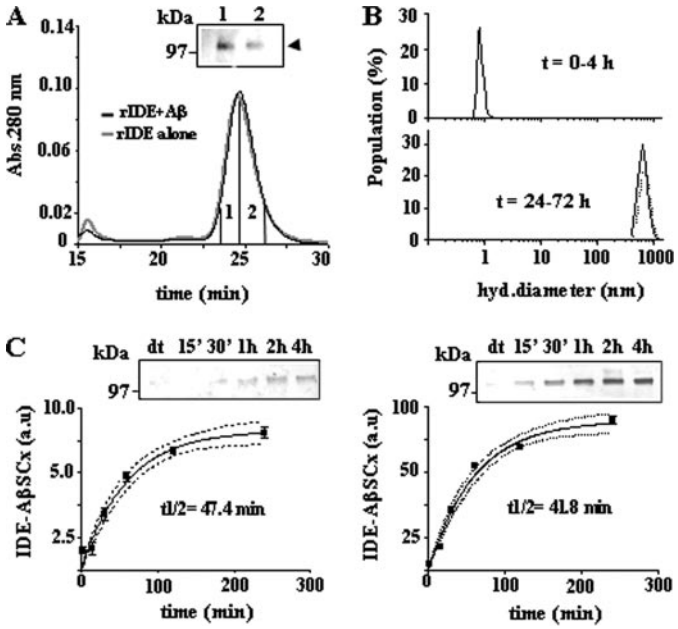

FIGURE 5. *A*, separation of IDE·AβSCx under native conditions on a Superdex 200 column. *Inset*, Western blot with 4G8 of *fractions 1* and *2*, as indicated. *B*, dynamic light scattering of Aβ1–28 pre-treated with HFIP, dissolved in 0.1 M phosphate, pH 7.2, at 100 μM and incubated for the indicated times at 37 °C. The relative abundance of species and the average hydrodynamic (*hyd.*) diameter in Log_{10} nm are shown for each incubation period. *C*, time course of rIDE·AβSCx formation under pseudo-first order conditions assessed by Western blot with 6E10 (*inset*) without EDTA (*left panel*) and after Zn^{2+} chelation with 5 mM EDTA (*right panel*). Densitometric data from two independent experiments in duplicate were fit to a single exponential equation. 95% confidence intervals are depicted. Note that both membranes (with or without EDTA experiments) were developed simultaneously with the STORM 860 scanner.

shown). At this rIDE concentration, no monomer was detected. Using [^{125}I]insulin as a substrate, >95% of the proteolytic activity was associated with the dimeric component (V_{max} = 3.9 fmol/h/μg) (not shown) indicating that our active recombinant protease had a quaternary structure similar to the native mammalian enzyme. After incubation with Aβ1–28, Western blot showed the presence of a 120-kDa band recognized by 4G8 that co-eluted with the rIDE-containing fractions (Fig. 5*A*). This band was not seen when Aβ1–28 was incubated alone (not shown), indicating that IDE·AβSCx was formed under non-denaturing conditions, and that native IDE·AβSCx had a similar molecular mass as rIDE, in accordance with the SDS-PAGE results described before. Because the hydrophobic region Aβ29–40 was not necessary for IDE·AβSCx assembly, we used Aβ1–28 instead of full-length Aβs to follow the time course of IDE·AβSCx formation. This allowed us to use a high peptide: enzyme molar ratio to ensure pseudo-first order conditions while minimizing the rate of Aβ aggregation. Moreover, MALDI-TOF analysis showed that after incubation with rIDE, Aβ1–28 was cleaved mainly at His^{13}-His^{14} and His^{14}-Gln^{15}, and therefore it was an rIDE substrate with a similar specificity as Aβ1–40 (12) (supplemental Fig. S4). Aβ1–28 was previously treated with HFIP, and its aggregation was monitored by dynamic light scattering. At 100 μM, Aβ1–28 remained as a predominant species of ~1 nm, consistent with monomeric peptide up to 4 h. After 24- and 72-h incubation, large oligomers became evident with apparent hydrodynamic diameters of 300 to ~600 nm, respectively (Fig. 5*B*). A time course of IDE·AβSCx formation between rIDE and Aβ1–28 under a 100-fold molar excess of peptide showed that it was a very slow process that approached steady state at 4 h. Fitting the data to a single exponential equation yielded an apparent rate constant, k = 0.015 min^{-}1 with $t_{½}$ of 47.4 min. When rIDE proteolytic activity was inhibited with EDTA, there was a substantial increase (~10-fold) in the amount of IDE·AβSCx formed yet with a similar rate (k = 0.017 min^{-}1) and $t_{½}$ (~42 min) (Fig. 5*C*).

Formation of IDE·AβSCx Is Prevented by Partial Denaturation and Competed by IDE Substrates—We next explored if soluble Aβ could be binding to rIDE in a substrate-like manner before IDE·AβSCx was formed. Because binding of Aβ and other substrates requires a natively folded IDE (14), we first studied whether rIDE denaturation affected the formation of IDE·AβSCx. When rIDE was incubated with increasing urea concentrations, a gradual decrease of molar ellipticity at 222 nm and a red shift of Trp fluorescence were indicative of a loss of secondary and tertiary structure, respectively, upon denaturation (Fig. 6*A*). Next, rIDE was incubated with Aβ1–28 under native conditions or in the presence of increasing concentrations of urea. A substantial reduction of the yield of IDE·AβSCx was evident between 2 and 3 M urea and remained at basal levels thereafter (Fig. 6*A*). To extend these results to the shorter Aβ17–27, FAβ (supplemental Fig. S3) was incubated with rIDE with and without prior incubation of the enzyme with 8 M urea. The yield of IDE·AβSCx under native conditions was 9-fold higher as compared with denatured rIDE. These results suggested that partially unfolded rIDE was inefficient in forming a stable complex with Aβ or that the presence of urea prevented the interaction of Aβ with rIDE (Fig. 6*B*). To gain information about the possible binding site on rIDE, competition was performed with insulin, the substrate with the lowest K_m for IDE (32). When insulin was incubated with rIDE at increasing concentrations for 1 h before the addition of FAβ, the yield of IDE·AβSCx approached a plateau at ~20% of the initial value in the absence of insulin (Fig. 6*C*). The lack of a total displacement by high concentrations of insulin and the fact that insulin was ineffective to displace FAβ when incubated after completion (4 h) of IDE·AβSCx formation (not shown) was indicative of a population of rIDE·Aβ that were not in equilibrium, in accordance with its high resistance to denaturation. Similar results were obtained when GRF, a known substrate of IDE, was used (32) (Fig. 6*D*). These results suggested the interaction of Aβ17–27 with at least part of a substrate binding site of IDE as an early step in IDE·AβSCx formation.

Peptides from the Catalytic Domain of IDE Are Tightly Associated with Aβ—The previous set of results was consistent with an encounter complex between monomeric Aβ and at least part of the substrate binding site of IDE followed by a slow transition leading to IDE·AβSCx. To determine which region of rIDE was associated with FAβ in a denaturant-resistant manner, IDE·AβSCx was subjected to partial proteolysis with trypsin, separated on SDS-PAGE, and analyzed by protein staining, fluorescence, and Western blot. Coomassie Blue revealed a broad band of ~25-kDa band that was not present in the undigested sample. Its N-terminal sequence from a PVDF membrane

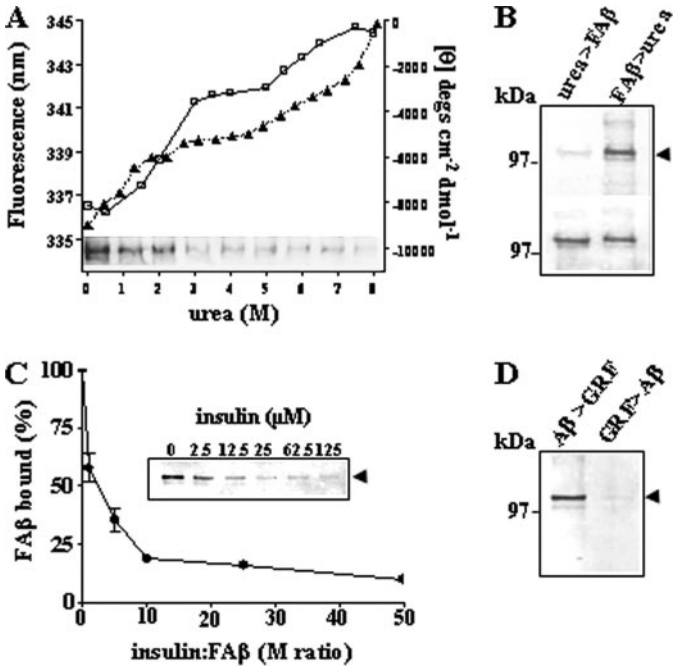

FIGURE 6. *A*, chemical denaturation of rIDE, as assessed by Trp fluorescence center of spectral mass (□) and loss of molar ellipticity at 222 nm (▲). rIDE was incubated in 50 mM phosphate buffer, pH 7.2, at room temperature in the presence of the indicated concentrations of urea for 1 h and then incubated with Aβ1–28 for 3 h at 37 °C. *Inset*: Western blot with 6E10 of IDE·AβSCx at the indicated urea concentrations. *B*, effect of 8 M urea upon the yield of FAβ-rIDE SDS-resistant complex applied to rIDE before incubation with the peptide (*urea > FAβ*) or after the complex was formed (*FAβ > urea*). Fluorescence scan (*top*) and Coomassie Blue staining of the same membrane (*bottom*) to show rIDE amounts. *C*, IDE·AβSCx was competed when the enzyme was preincubated for 1 h with increasing concentrations of insulin. Data were plotted as the percentage of remaining 120-kDa complex as a function of insulin:FAβ molar ratio. Points represent the mean ± S.E. of three independent experiments. *Inset*: fluorescence detection of bound FAβ. *D*, fluorescence detection of FAβ after SDS-PAGE shows that incubation of rIDE with an excess of GRF for 1 h before the addition of FAβ prevents IDE·AβSCx formation (*GRF > Aβ*). There is no displacement of FAβ after IDE·AβSCx was formed (*Aβ > GRF*).

yielded 1.5 pmol of a major Ser-Met-Asn-Asn-Pro-Ala-Ile, starting at the last residue of the pET expression vector. A fluorescent and 4G8-immunoreactive band was consistent with FAβ bound to this rIDE product (Fig. 7*A*). To gain more structural information with a different approach, IDE·AβSCx was formed with FAβCys17–27 (which lacks Lys^{16} and Lys^{28}), the band of 120 kDa was cut and digested in gel with endo-LysC. The products were separated by reversed-phase HPLC and assessed for 4G8 immunoreactivity and fluorescence (Fig. 7*B*). Five fractions were analyzed by MALDI-TOF, according to the presence of both criteria, numbered 36c, 37c, 39c, 40c, and 41c, respectively. The complete list of endo-LysC fragments that were assigned to rIDE from these fractions is provided as supplemental material in Table S1. The most frequent IDE peptides recovered from IDE·AβSCx as compared with rIDE alone were clustered within region 57–131 (supplemental Fig. S5 and supplemental Table S1). In the absence of an obvious candidate peptide for an Aβ adduct (not expected to resist MALDI-TOF if not covalent), a frequency distribution of peptides within 100-residue segments of IDE was done. A total of 200 peptides that co-eluted with FAβ17–27 were assignable to rIDE, of which ~15% mapped to the region 51–150 of the protease, a 4-fold over-representation as compared with the peptides obtained in the same fractions from rIDE alone (3.5%) (Fig. 7*C*).

DISCUSSION

Our results indicate that a region of IDE containing the catalytic site is capable of an extremely stable association with Aβ without prior cleavage of the peptide. Several proteins have been shown to interact with Aβ in a manner that is resistant to SDS, including apolipoprotein E isoforms, apolipoprotein J, α2-macroglobulin (α2M), transthyretin, gelsolin, and the α7-nicotinic acetylcholine receptor subunit (33–38). Some of these proteins, like IDE, have been found in close association with or within amyloid plaques in AD brains (28).[4] The best studied binding requirements were those of the apolipoprotein E·Aβ complex, showing that the N-terminal region of Aβ His^{13}–Lys^{16} may interact with the C terminus of the peptide for the strong binding to a natively folded apolipoprotein E (34). This same region of Aβ has been involved in the binding to transthyretin, possibly through charge interactions (36). The shortest Aβ fragment used in this study (positions 17–27) that was competent to interact with IDE in a stable manner contained the sequence LVFF, known to be important in driving β-sheet formation (30, 39, 40). The Aβ sequence 17–21 (LVFFA) has been shown to form a surface hydrophobic patch in the metastable "collapsed coil" of Aβ10–35 in water (41), whereas the Aβ16–28 stretch forms a β strand that may drive the intermolecular association of fibrillar Aβ (42). Moreover, the recently resolved three-dimensional structure of an inactive IDE mutant (E111Q) complexed with several substrate peptides shows that this central stretch (residues 16–23) of Aβ binds in an extended conformation within the catalytic cleft of IDE (14). Apart from wild-type Aβ, synthetic and endogenous Aβ Dutch also bound tightly to IDE, indicating that a negative charge at residue 22 was not necessary for such interaction. The kinetic of IDE·AβSCx formation under pseudo-first order conditions revealed that it was a very slow process and that its yield was increased when IDE activity was inhibited by removing catalytic Zn^{2+} with chelators. Together with the fact that Aβ1–28 remained largely monomeric throughout the incubation period, these results suggested three major possibilities: 1) IDE·AβSCx derived from an encounter complex between substrate and a fully active protease via a pathway that was alternative to proteolysis, 2) IDE·AβSCx was generated exclusively by a population of rIDE molecules with a very slow k_{cat} or with no catalytic activity (*i.e.* due to conformational changes or the absence of Zn^{2+}), and 3) Aβ occupied a region in IDE that overlapped only partially with the canonic binding site and therefore catalytically inactive. The study of the kinetic of inhibition using very sensitive IDE substrates comparing free IDE and IDE·AβSCx will help to decide between these alternatives and allow a more in-depth mechanistic interpretation. Our results indicate that monomeric or very low order oligomers of Aβ and a natively folded IDE were the competent species for the assembly of IDE·AβSCx. IDE·AβSCx was strongly competed out when IDE was preincubated with two good IDE substrates such as insulin and GRF. The facts that competition was not

[4] V. Dorfman and L. Morelli, unpublished observations.

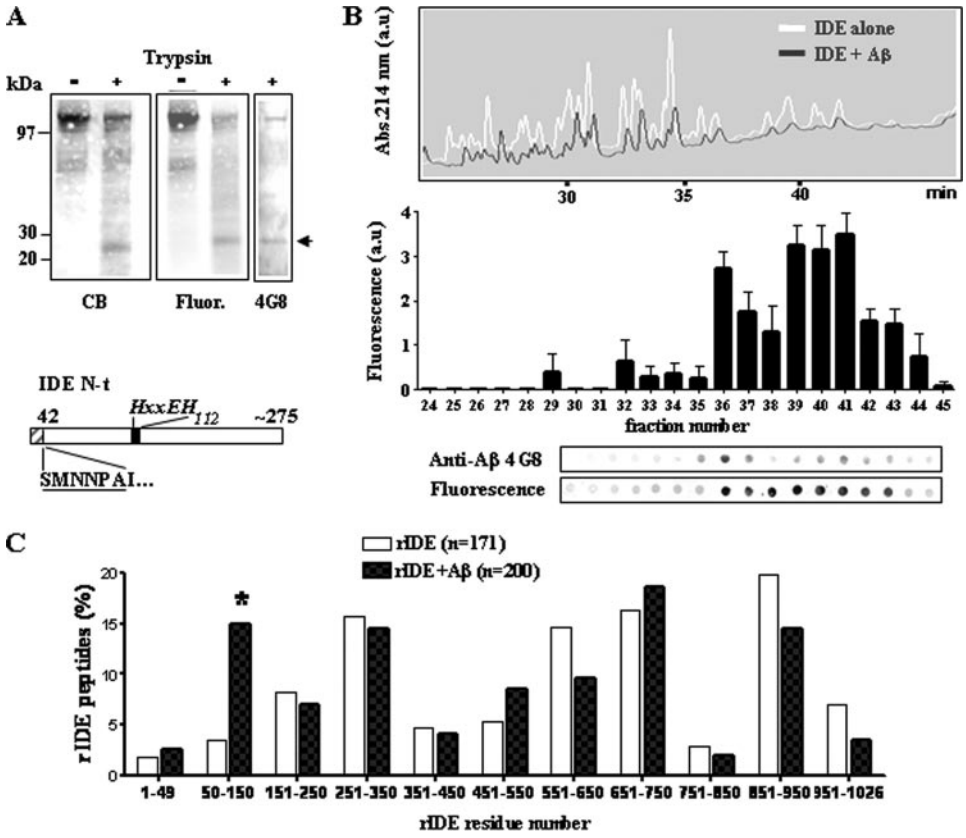

FIGURE 7. *A*, *top panel*, Coomassie blue (*CB*) staining, fluorescence, and Western blot with 4G8 of rIDE after incubation with FAβ, undigested and partially digested with trypsin, as indicated. The *arrow* shows FAβ bound to a 25-kDa tryptic rIDE fragment. *Bottom panel*, schematic representation of the N-terminal domain of rat IDE (*IDE N-t*) showing the N-terminal sequence obtained from the 25-kDa tryptic fragment. Residues involved in catalysis are depicted in *italics*. Numbering follows the full-length cDNA of rat IDE. *B*, *top panel*, HPLC profiles of the in-gel endo-LysC digestion of rIDE alone or preincubated with FAβ17–27. *Bottom panel*, fluorescence and Aβ immunoreactivity of the HPLC fractions after in gel digestion of IDE·AβSCx. *Bars* represent the mean ± S.E. of duplicates from two independent experiments. *C*, frequency distribution of all the endo-LysC peptides derived from fractions 36, 37, 39, 40, and 41 that were assigned to rIDE sequence from two independent experiments performed in duplicate. *Open bars*, rIDE alone; *filled bars*, rIDE incubated with FAβ17–27. The *asterisk* indicates the 4-fold over-representation of peptides from the region 51–150 of rIDE. Note that the numbering refers to our recombinant IDE and that the N-terminal 49 residues are from the pET sequence.

complete and that there was no displacement of Aβ when IDE·AβSCx was allowed to form before the addition of competitor were concurrent with a non-equilibrium reaction between Aβ and rIDE. Our limited proteolysis and mass spectrometry findings fully agreed with the competition experiments, showing that IDE peptides within the catalytic domain were preferentially retrieved after HPLC in tight association with Aβ17–27. Collectively, these results suggest that monomeric Aβ interacts with part of the substrate-binding site of IDE to yield, via a slow rearrangement, the irreversible peptide·protease complex. Kurochkin (11) has proposed that the substrate specificity of IDE is realized at the binding stage, a step in which the protease "senses" the potential of the peptide to adopt an extended β conformation by providing a template that promotes this conversion. The spatial distribution of insulin B chain, amylin, glucagon, and Aβ1–40 associated with an inactive mutant of IDE fully supports such mechanism (14). Self-assembly of amyloidogenic peptides usually results in very stable end products that can resist harsh chemical denaturation. As a remarkable example *in vivo*, soluble neurotoxic Aβ oligomers of 56 kDa found in the brains of APP transgenic mice, completely resisted denaturation with 8 M urea, whereas smaller Aβ oligomers resisted treatment with HFIP (43). The extended conformation of Aβ16–23 in its IDE-bound form (14) and the biochemical data presented here raise the intriguing possibility that the tight association between IDE and Aβ, despite being heterologous, may share thermodynamic and structural features with the self-assembly of amyloid peptides. *In vitro* seeding experiments of amylin with Aβ fibrils partially support this possibility (44). The occurrence of a covalent binding between rIDE and Aβ cannot be excluded completely, yet, there are no covalent intermediates of amide hydrolysis by metallopeptidases as opposed to serine or cysteine proteases (45) and the removal of catalytic Zn^{2+} greatly enhanced IDE·AβSCx formation, pointing to a non-catalytic-dependent mechanism. The high conservation of IDE, together with the convergent evolution of the catalytic fold of Zn^{2+}-metallopeptidases such as thermolysin and neprilysin, suggests that a common strategy has prevailed for the degradation of peptides prone to adopt an extended conformation (46, 47). IDE, in addition to its function as an insulin peptidase, may act in cellular and extracellular compartments as a scavenger of peptides with a high propensity to form β aggregates by degrading them at a monomeric stage. Nonetheless, the present results tempt us to speculate that an irreversible, non-catalytic binding may represent an alternative to trap metastable peptides before they reach a critical concentration that would promote nucleation and render them less accessible to proteolysis *in vivo*. It remains as a testable prediction for further investigation whether IDE is capable of forming stable complexes with other amyloidogenic peptides besides Aβ. This type of interaction may be a general property of IDE and may acquire pathogenic importance in the context of tissue specificity of amyloid accumulation. In the case of the AD brain, a stoichiometric irreversible complex involving Aβ and a "suicide" conformer of IDE that enters a dead-end pathway may compromise insulin turnover and promote local insulin resistance under conditions in which Aβ is produced at a high rate such as during cellular hypoxic stress (48). Moreover, the sensitivity of IDE to oxidative damage (21, 22) may reduce its catalytic activity and further promote the formation of IDE·AβSCx. In the case of Aβ1–40, the apparent K_m for IDE is 0.8–2 μM (18, 49) and the reported critical concentration varies from ~1 to 20 μM (50, 51) thus

making the system highly sensitive to Aβ overproduction and/or accumulation with regard to the degradation-aggregation balance. This may also be relevant to the most abundant product of APP processing by α/γ secretases, the p3 peptides that contain the sequence 17–27 of Aβ and are a major component of diffuse plaques in AD (52, 53). In summary, our results raise the possibility of a novel conformation-dependent interaction between IDE and Aβ peptide substrates with potential pathogenic implications in sporadic AD and related disorders.

REFERENCES

1. Morelli, L., Llovera, R., Ibendhal, S., and Castaño, E. M. (2002) *Neurochem. Res.* **27,** 1387–1399
2. Harper, J. D., and Lansbury, P. T., Jr. (1997) *Annu. Rev. Biochem.* **66,** 385–407
3. Iwata, N., Tsubuki, S., Takaki, Y., Shirotani, K., Lu, B., Gerard, N. P., Gerard, C., Hama, E., Lee, H. J., and Saido, T. C. (2001) *Science* **292,** 1550–1552
4. Farris, W., Mansourian, S., Chang, Y., Lindsley, L., Eckman, E. A., Frosch, M. P., Eckman, C. B., Tanzi, R. E., Selkoe, D. J., and Guenette, S. (2003) *Proc. Natl. Acad. Sci. U. S. A.* **100,** 4162–4167
5. Miller, B. C., Eckman, E. A., Sambamurti, K., Dobbs, N., Chow, K. M., Eckman, C. B., Hersh, L. B., and Thiele, D. L. (2003) *Proc. Natl. Acad. Sci. U. S. A.* **100,** 6221–6226
6. Eckman, E. A., Watson, M., Marlow, L., Sambamurti, K., and Eckman, C. B. (2003) *J. Biol. Chem.* **278,** 2081–2084
7. Leissring, M. A., Farris, W., Chang, A. Y., Walsh, D. M., Wu, X., Sun, X., Frosch, M. P., and Selkoe, D. J. (2003) *Neuron* **40,** 1087–1093
8. Roth, R (2004) in *Handbook of Proteolytic Enzymes* (Barrett, A. J., Rawlings, N. D., and Woessner, J. F., eds) pp. 868–876, Elsevier Academic Press, New York
9. Qiu, W. Q., Walsh, D. M., Ye, Z., Vekrellis, K., Zhang, J., Podlisny, M. B., Rosner, M. R., Safavi, A., Hersh, L. B., and Selkoe, D. J. (1998) *J. Biol. Chem.* **273,** 32730–32738
10. Sudoh, S., Frosch, M. P., and Wolf, B. A. (2002) *Biochemistry* **41,** 1091–1099
11. Kurochkin, I. V. (2001) *Trends Biochem. Sci.* **26,** 421–425
12. Morelli, L., Llovera, R., Gonzalez, S. A., Affranchino, J. L., Prelli, F., Frangione, B., Ghiso, J., and Castaño, E. M. (2003) *J. Biol. Chem.* **278,** 23221–23226
13. Morelli, L., Llovera, R. E., Alonso, L. G., Frangione, B., de Prat Gay, G., Ghiso, J., and Castaño, E. M. (2005) *Biochem. Biophys. Res. Commun.* **332,** 808–816
14. Shen, Y., Joachimiak, A., Rosner, M. R., and Tang, W. J. (2006) *Nature* **443,** 870–887
15. Vepsalainen, S., Parkinson, M., Helisalmi, S., Mannermaa, A., Soininen, H., Tanzi, R., Bertram, L., and Hiltunen, M. (2007) *J. Med. Genet.* **44,** 606–608
16. Qiu, W. Q., and Folstein, M. F. (2006) *Neurobiol. Aging* **27,** 190–198
17. Luchsinger, J. A., Tang, M. X., Shea, S., and Mayeux, R. (2004) *Neurology* **63,** 1187–1192
18. Pérez, A., Morelli, L., Cresto, J. C., and Castaño, E. M. (2000) *Neurochem. Res.* **25,** 247–255
19. Cook, D. G., Leverenz, J. B., McMillan, P. J., Kulstad, J. J., Ericksen, S., Roth, R. A., Schellenberg, G. D., Jin, L. W., Kovacina, K. S., and Craft, S. (2003) *Am. J. Pathol.* **162,** 313–319
20. Morelli, L., Llovera, R. E., Mathov, I., Lue, L., Frangione, B., Ghiso, J., and Castaño, E. M. (2004) *J. Biol. Chem.* **279,** 56004–56013
21. Shinall, H., Song, E. S., and Hersh, L. B. (2005) *Biochemistry* **44,** 15345–15350
22. Caccamo, A., Oddo, S., Sugarman, M. C., Akbari, Y., and LaFerla, F. M. (2005) *Neurobiol. Aging* **26,** 645–654
23. Castaño, E. M., Prelli, F., Soto, C., Beavis, R., Matsubara, E., Shoji, M., and Frangione, B. (1996) *J. Biol. Chem.* **271,** 32185–32191
24. Wood, S. J., Maleeff, B., Hart, T., and Wetzel, R. (1996) *J. Mol. Biol.* **256,** 870–877
25. Saric, T., Muller, D., Seitz, H. J., and Pavelic, K. (2003) *Mol. Cell. Endocrinol.* **204,** 11–20
26. Wisniewski, H. M., Wen, G. Y., and Kim, K. S. (1989) *Acta Neuropathol. (Berl.)* **78,** 22–27
27. Harigaya, Y., Shoji, M., Kawarabayashi, T., Kanai, M., Nakamura, T., Iizuka, T., Igeta, Y., Saido, T. C., Sahara, N., Mori, H., and Hirai, S. (1995) *Biochem. Biophys. Res. Commun.* **211,** 1015–1022
28. Bernstein, H. G., Ansorge, S., Riederer, P., Reiser, M., Frolich, L., and Bogerts, B. (1999) *Neurosci. Lett.* **263,** 161–164
29. Gorevic, P. D., Castaño, E. M., Sarma, R., and Frangione, B. (1987) *Biochem. Biophys. Res. Commun.* **147,** 854–862
30. Liu, R., Yuan, B., Emadi, S., Zameer, A., Schulz, P., McAllister, C., Lyubchenko, Y., Goud, G., and Sierks, M. R. (2004) *Biochemistry* **43,** 6959–6967
31. Shii, K., Yokono, K., Baba, S., and Roth, R. A. (1986) *Diabetes* **35,** 675–683
32. Safavi, A., Miller, B. C., Cottam, L., and Hersh, L. B. (1996) *Biochemistry* **35,** 14318–14325
33. Strittmatter, W. J., Saunders, A. M., Schmechel, D., Pericak-Vance, M., Enghild, J., Salvesen, G. S., and Roses, A. D. (1993) *Proc. Natl. Acad. Sci. U. S. A.* **90,** 1977–1981
34. Munson, G. W., Roher, A. E., Kuo, Y. M., Gilligan, S. M., Reardon, C. A., Getz, G. S., and LaDu, M. J. (2000) *Biochemistry* **39,** 16119–16124
35. Hughes, S. R., Khorkova, O., Goyal, S., Knaeblein, J., Heroux, J., Riedel, N. G., and Sahasrabudhe, S. (1998) *Proc. Natl. Acad. Sci. U. S. A.* **95,** 3275–3280
36. Schwarzman, A. L., Gregori, L., Vitek, M. P., Lyubski, S., Strittmatter, W. J., Enghilde, J. J., Bhasin, R., Silverman J., Weisgraber, K. H., Coyle, P. K., Zagorski, M. G., Talafous, J., Eisenberg, M., Saunders, A. M., Roses, A. D., and Goldgaber, D. (1994) *Proc. Natl. Acad. Sci. U. S. A.* **91,** 8368–8372
37. Chauhan, V. P., Ray, I., Chauhan, A., and Wisniewski, H. M. (1999) *Biochem. Biophys. Res. Commun.* **258,** 241–246
38. Wang, H. Y., Lee, D. H., D'Andrea, M. R., Peterson, P. A., Shank, R. P., and Reitz, A. B. (2000) *J. Biol. Chem.* **275,** 5626–5632
39. Hilbich, C., Kisters-Woike, B., Reed, J., Masters, C. L., and Beyreuther, K. (1992) *J. Mol. Biol.* **228,** 460–473
40. Soto, C., Sigurdsson, E. M., Morelli, L., Kumar, R. A., Castaño, E. M., and Frangione, B. (1998) *Nat. Med.* **4,** 822–826
41. Zhang, S., Iwata, K., Lachenmann, M. J., Peng, J. W., Li, S., Stimson, E. R., Lu, Y., Felix, A. M., Maggio, J. E., and Lee, J. P. (2000) *J. Struct. Biol.* **130,** 130–141
42. Luhrs, T., Ritter, C., Adrian, M., Riek-Loher, D., Bohrmann, B., Dobeli, H., Schubert, D., and Riek, R. (2005) *Proc. Natl. Acad. Sci. U. S. A.* **102,** 17342–17347
43. Lesne, S., Koh, M. T., Kotilinek, L., Kayed, R., Glabe, C. G., Yang, A., Gallagher, M., and Ashe, K. H. (2006) *Nature* **440,** 352–357
44. O'Nuallain, B., Williams, A. D., Westermark, P., and Wetzel, R. (2004) *J. Biol. Chem.* **279,** 17490–17499
45. Auld, D. S. (2004) in *Handbook of Proteolytic Enzymes* (Barrett, A. J., Rawlings, N. D., and Woessner, J. F., eds) pp. 268–289, Elsevier Academic Press, New York
46. Makarova, K. S., and Grishin, N. V. (1999) *Protein Sci.* **8,** 2537–2540
47. Oefner, C., D'Arcy, A., Hennig, M., Winkler, F. K., and Dale, G. E. (2000) *J. Mol. Biol.* **296,** 341–349
48. Wang, R., Zhang, Y. W., Zhang, X., Liu, R., Zhang, X., Hong, S., Xia, K., Xia, J., Zhang, Z., and Xu, H. (2006) *FASEB J.* **20,** 1275–1287
49. Leissring, M. A., Lu, A., Condron, M. M., Teplow, D. B., Stein, R. L., Farris, W., and Selkoe, D. J. (2003) *J. Biol. Chem.* **278,** 37314–37320
50. O' Nuallain, B., Shivaprasad, S., Kheterpal, I., and Wetzel, R. (2005) *Biochemistry* **44,** 12709–12718
51. Chen, Y. R., and Glabe, C. G. (2006) *J. Biol. Chem.* **281,** 24414–24422
52. Esch, F. S., Keim, P. S., Beattie, E. C., Blacher, R. W., Culwell, A. R., Oltersdorf, T., McClure, D., and Ward, P. J. (1990) *Science* **248,** 1122–1124
53. Gowing, E., Roher, A. E., Woods, A. S., Cotter, R. J., Chaney, M., Little, S. P., and Ball, M. J. (1994) *J. Biol. Chem.* **269,** 10987–10990